# Production of Surface Acoustic Wave Resonator Using Laser Ablation Method and Its Finite Element Modeling

Alexander Kukaev, Daniil Safronov, Vladislav Sheroshenko

Saint-Petersburg Electrotechnical University
Saint Petersburg, Russia
ASKukaev@gmail.com

*Abstract*—**Surface acoustic wave (SAW) gyroscopes have a lot of advantages, such as small size, low price, high shock and vibration resistance and others. Nowadays its research is moving slowly because optimization of these sensors construction requires quick prototyping, which is impossible if we use traditional photolithography techniques. A novel method of laser topology creation was previously proposed to mind this gap. In this work, the first SAW resonator was created using this method. Its characteristics were studied. In addition, a finite element modeling of gyroscope sensing element of this type was performed to find out the potential sensors characteristic.**

## I. Introduction

Nowadays popularity of sensors based on surface acoustic waves (SAW) is rising. These sensors are comparable with MEMS in size, price and sensitivity characteristics, but also include such unique advantages as high shock resistance and possibility of a wireless sensing. Many different design concepts of SAW-based gyroscopes were proposed in a recent decade [1–3]. Generally, they might be divided into two groups: on running and on standing waves (some of them utilize both). Each of them have some specific features and advantages along with specifics in production and simulation. Main differences are in its topologies. Therefore, formation of electrode topology on a surface of a wafer is a key part of SAW-based sensor fabrication process and mostly determines its sensitivity characteristics.

Originally, a photolithography method is used for electrode topology creation. However, modern design concepts of solid-state inertial sensors (gyroscopes, accelerometers) have complicated topology that may contain several delay lines, resonators and other elements on a single wafer [4, 5]. Production of a photo mask for its etching is a difficult and expensive process. It becomes crucial in case of small series that are needed at the development stage for optimization purposes – every small change in topology requires a new photomask. In addition, a life cycle of these masks is comparatively short. Therefore, a method of drawing a sensitive element topology using a high-precision laser seems perspective [6, 7]. The essence of proposed method is to evaporate unneeded material from a fully metallized wafer, leaving only desired topology. In this case, there is no need to produce a photo mask. Thus, it is possible to change sensing element configuration without any essential expenses of time

and money that will allow simplifying technological process of SAW-based sensors production.

Frequency of a SAW resonator is dependent on a width of the interdigital transducers (IDT) fingers and the distance between them:

$$\lambda = \frac{V}{f_0} \; ; \; h = \frac{\lambda}{2} \; ; \; d = \frac{\lambda}{4},$$

where $\lambda$ is a length of the acoustic wave, $V$ is a SAW propagation velocity, $f_0$ is a SAW frequency, $h$ is a distance between neighboring electrodes, $d$ is a width of the electrode. Therefore, if the one could partially remove material from IDT fingers, then the frequency of the resonator will change by a known value. This operation may be performed using a focused laser beam.

The value, by which the one needs to adjust a resonator frequency, and, therefore, the amount of a material to be vapored, differs from resonator to resonator. In case of mass production, this approach does not look appropriate. Thus, it is more promising to perform the whole production procedure of a sensing element using a laser. In this case, the substrate of piezo crystal is preliminary covered with a thin metal layer. There is no limitations on the thickness of this layer. It can be from 0.2 to 20 μm thick if required by the terms of application[3]. Traditional method of etching cannot form a proper topology with this thickness (20 μm) due to a large taper of a formed structure.

Another advantage of the proposed method is the ease of new topologies formation in comparison with the photolithography method, in which you have to create a special expensive mask to produce a new topology. It is especially important in a small series production. Next, the number of production steps is reduced that increases the production rate. In addition, using of optically transparent acoustic line (quartz for example) allows us to create a topology on both sides simultaneously. However, we must take into account the way of laser beam positioning.

In previous works on progress in laser ablation method application for SAW-based sensors production only simple delay lines were produced and tested. In this paper we discuss the first attempt to produce a SAW resonator with a

complicated topology, suitable for application as a gyroscope sensing element. First, let us discuss its operation principle.

## II.  II. SAW-BASED GYRO ON STANDING WAVES

In 1997 M. Kurosawa et al. have proposed one of the first concepts of SSG based on standing SAWs [8, 9]. In this scheme the informative parameter is the amplitude of the secondary SAW. It is determined by the value of the Coriolis force. Fig. 1 a illustrates a standing SAW which is a superposition of two waves that travel in opposite directions. Particles in its antinodes undergo vibrational motion in the direction perpendicular to the plane of the substrate, and in the nodes they oscillate in it. The oscillations provide an opportunity to excite the Coriolis force during rotation and, consequently, determine the value of angular velocity (Fig. 1 b).
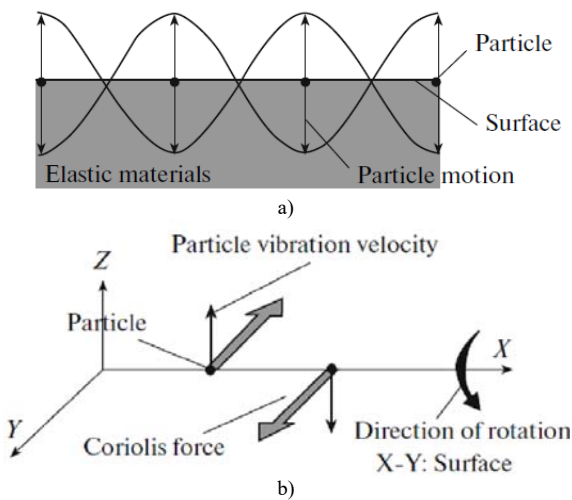


a)



b)

Fig. 1. The motion of particles in standing Rayleigh waves:a) In the absence of rotation, and b) during rotation

Excited Coriolis force is proportional to the mass of moving substrate particles. Therefore, the amplitude of the secondary wave is believed to be too small to be detected. For this reason, the authors propose to place a matrix of miniature inertial masses (66×61 mm, $1.5 \cdot 10^{-11}$ g) in the resonator cavity. The block diagram of this sensor is shown in Fig. 2.
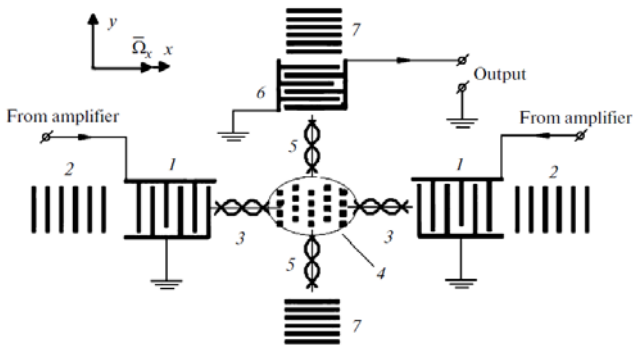


Fig. 2. SAW-based SSG with a matrix of distributed inertial masses

Here the primary standing wave 3 is generated by exciting IDTs 1 and reflectors 2. Miniature masses 4 form the matrix in

the antinodes of the primary wave.  With the particles of the substrate they oscillate along the z-axis.  In the presence of angular velocity (Fig. 2), the Coriolis acceleration and the corresponding force act in the direction orthogonal to the primary wave 3. Under its influence the substrate particles together with inertial masses undergo vibrational motion along the y-direction, exciting the secondary SAW 5, which is detected by the secondary resonator formed by IDT 6 and reflectors 7.

Later described concept had several modifications [4, 10], but may be considered as a basic one as it includes most of common elements in its design (IDTs, reflectors, tiny inertial masses). Therefore, it is promising to test a novel fabrication method on this design.

## III.  PRODUCTION OF SURFACE ACOUSTIC WAVE RESONATOR USING LASER ABLATION METHOD

A round wafer of 128° YX $LiNbO_3$ with a diameter of 3 inches covered with 50 nm of copper was used as a die for further processing. A "MiniMarker 2"precision laser engraver [11] with a fiber transmitter was used to draw a desired topology. Existing lens was limiting the possible frequency of a SAW resonator from above, so it was designed to have a central frequency of 16.49 MHz. Photo of produced sensing element prototype is shown in Fig. 3.
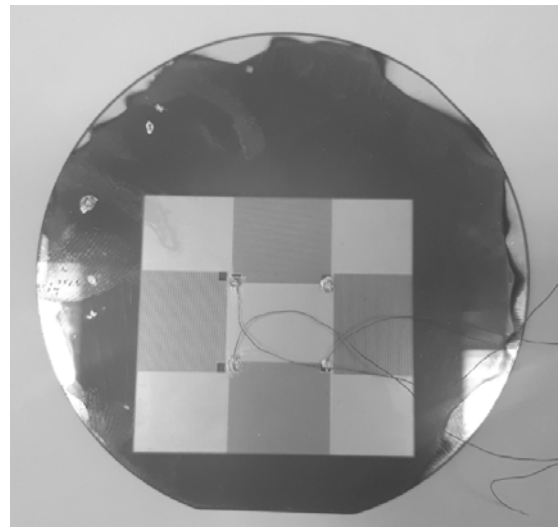


Fig. 3. Produced sensing element prototype

To investigate a quality of produced structure series of photos were made using an optical microscope (Fig. 4). It is seen that reflectors are of a good quality: straight, with equal width and spacing, without visible defects.

Square inertial masses with the edge size of λ/4 were measured using a special microscope software. The difference in its size along x and y axes was not more than 0.2–0.3 μm. This indicates that the laser regime was chosen correctly. White blurred lines at the top and bottom of the inertial masses are also noticeable. Their presence is due to the fact that the laser beam moved from top to bottom. In places where the inertial mass should be located, the laser was turned off and then, after turning the mirror of the scanner after the inertial mass, it
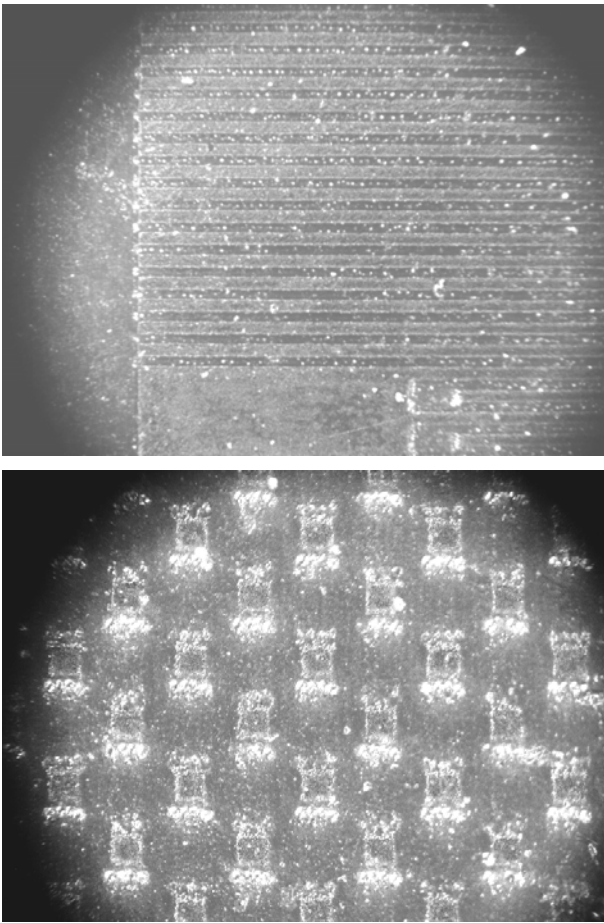
Fig. 4. Microphotos of produced prototype: reflectors and IDT (above) and inertial masses matrix (below)

turned on again. At the places of switching on and off, the mirror of the scanner slows down and accelerates. In this connection, the areas are exposed for a longer time. Theoretically, this can lead to a worsening of acoustic wave propagation. However, in practice, these impairments may not be significant. To assess the operability of the obtained sample, it is necessary to estimate its spectral characteristics.

Produced prototype was tested on the spectrum analyzer. Obtained frequency curve of a primary resonator is shown in Fig. 5.
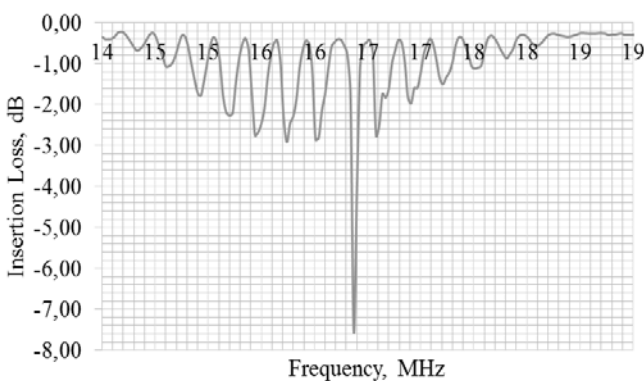


Fig. 5. Spectrum of a primary resonator

As can be seen from this image, the resonance peak occurs at a frequency of 16.37 MHz, with a desired frequency of 16.49 MHz. Thus, the difference between the actual frequency and the estimated frequency is approximately 1%, which indicates a high quality of performance. In addition, the ratio of the central peak to the nearest harmonics is 2.68. As a result, it is possible to build a generator on the carrier frequency without introducing distortion from the side harmonics.

Proposed method of topology creation allows to quickly get the sensitive element of the navigation sensor. However, before the final device is built, it is necessary to calculate the electrical circuit, fabricate it, connect the sensor and install the prototype of the sensor on the turntable. All these steps are necessary to obtain the output characteristic, to estimate the scale factor, the zero drift, etc. However, before starting the production of prototypes, it is advisable to conduct a computer analysis of the future sensor. A computer model does not require the design of an electrical circuit. It is enough to build a model of a sensitive element, to set the necessary parameters for it and to conduct virtual tests. As a result of such tests it is possible to obtain the necessary characteristics of a SAW-based microgyroscope, and also to develop recommendations for their improvement.

IV. FINITE ELEMENT MODELING OF THE SENSING ELEMENT

OOFELIE::Multiphysics software was used for the simulation. Wave lengths propagating along two orthogonal axes were specified. The working frequency of the sensor had to be reduced to $f = 5.1$ MHz due to the limited computing power of the hardware. Increasing the frequency will complicate the process of calculation. The material of the wafer was chosen to be 128° YX LiNbO$_3$ with a SAW propagation velocity equal to 3960 m/s. Consequently, the wavelengths in different directions were equal to $\lambda_x = 790$ μm; $\lambda_y = 731$ μm. Fig. 6 shows the model basic geometry.
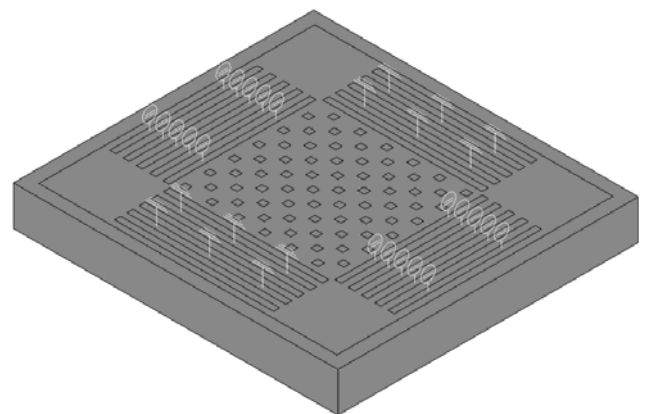


Fig. 6. A model built for FEM analyses

Piezoelectric crystal was surrounded by a perfectly matched layer (PML) that simulates a quasi-infinite medium and suppresses undesired reflections from the wafer edges. In the production of sensitive elements, the edges of the sound transmission line are treated in a special way so that the SAW is not re-reflected from them. To reduce the load on the computer, the real dimensions of the sensor were simplified,
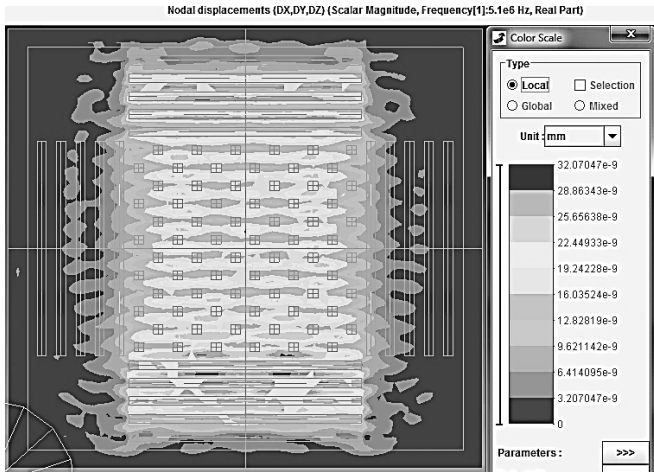
Fig. 7. Distribution of displacements without inertial masses and rotation
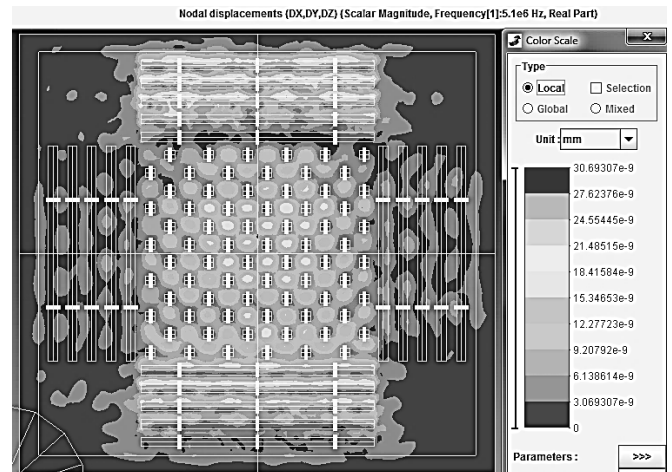


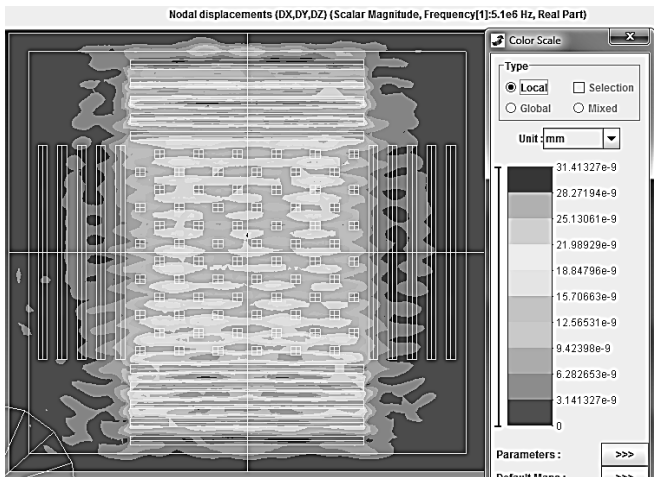Fig. 8. Distribution of displacements with inertial masses and without rotation



Fig. 9. Distribution of displacements without inertial masses and with rotation
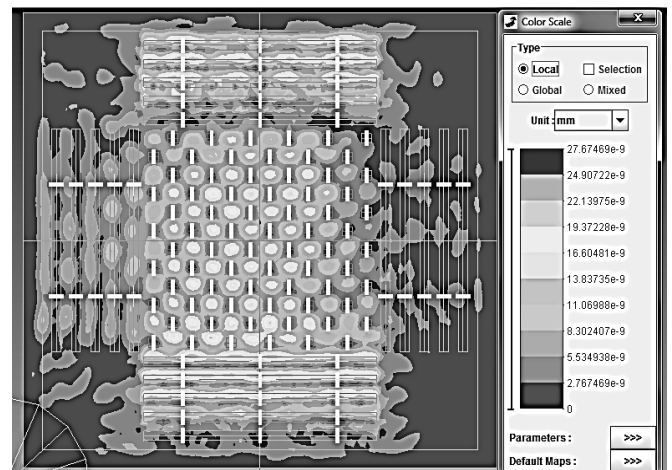


Fig. 10. Distribution of displacements with inertial masses and rotation

while the quality characteristics were not distorted due to the PML. A matrix of inertial masses organized in staggered order is located in the center of the crystal surface. The masses are positioned in the antinodes of the standing wave. When the wave propagates, the particles below the inertial masses will oscillate along elliptical trajectories, and the masses themselves will begin to oscillate along the Z axis.

IDTs were introduced as sets of 5 electrodes with a length of 5λ, width of λ/4 and spacing of λ/4. Half of them was grounded and the other part was loaded by electrical voltage of 1 V with a frequency of 5.1 MHz. Receiving electrodes with the same geometrical parameters were divided into two groups of equipotential faces. The model was meshed by parabolic tetrahedrons with an average edge length of 0.198 mm. The size comes from the idea of at least 8 finite elements per wavelength.

Fig. 7 shows particle displacements in the case of SAW propagation without inertial masses and angular velocity. In this case, the wave propagates uniformly over the surface and the displacement of the particles reaches values of $25.656 \cdot 10^{-9}$ mm. It is also easy to see that the SAW has a uniform distribution along the primary axis (axis of measurement, $x$ in Fig. 2).

Next, inertial masses were added to the model into the cavity region (Fig. 8). The propagation of the primary SAW was impeded by inertial masses located on its path. As a result, the displacement of particles decreases by 20% and is equal to $21.485 \cdot 10^{-9}$ mm. It should also be noted that there is a parasitic wave orthogonal to the primary one, which is caused by the scattering on inertial masses. Thus, in Fig. 8, it can be seen that in the state of rest there is a secondary wave propagating along horizontal axis and introducing a small displacement of the masses. Its presence can lead to a shift of zero. Now let us consider the cases of rotation of the model.

In the presence of angular velocity, the Coriolis effect arises, which initiates the displacement of the inertial masses in the direction orthogonal to the primary SAW propagation. Based on the requirements for solid-state navigation sensors, the rotation of the model was set at a speed of 100,000 deg/s. Fig. 9 shows the distribution of the acoustic wave in the absence of inertial masses, but with a stated angular velocity applied.

TABLE I. DEPENDENCE OF A GYRO SCALE FACTOR ON THE THICKNESS OF INERTIAL MASSES

| $h$, μm | 0,001 | 0.5 | 1 | 2 | 5 | 10 |
|---|---|---|---|---|---|---|
| Scale factor, V·rad·s$^{-1}$ | $1.14 \cdot 10^{-10}$ | $2.43 \cdot 10^{-10}$ | $3,77 \cdot 10^{-10}$ | $6.58 \cdot 10^{-10}$ | $1.64 \cdot 10^{-9}$ | $3.88 \cdot 10^{-9}$ |
| Inertial mass, kg | $7 \cdot 10^{-13}$ | $3.5 \cdot 10^{-10}$ | $7 \cdot 10^{-10}$ | $1.4 \cdot 10^{-9}$ | $3.5 \cdot 10^{-9}$ | $7 \cdot 10^{-9}$ |

Fig. 9 shows that in the presence of angular velocity, the picture did not change significantly. This is due to the small values of the mass of the particles of the wafer. As a consequence, the Coriolis force will tend to zero, and the energy of the primary wave will not go into the secondary wave even at very high angular velocities. The output characteristic of the prototype with this configuration is most likely to be absent.

A different picture is observed in the case where there are inertial masses in the cavity region (Fig. 10). Here the secondary wave has a harmonic distribution of displacements along the sound line. It is also easy to see that the intensity of displacements in the secondary channel has increased significantly in comparison with the case without inertial masses. Based on the obtained results, it can be concluded that with increasing inertial masses, the slope of the output characteristic of the solid-state SAW-based microgyroscope should increase, and its scale factor should increase as well. The next step was to evaluate these parameters and analyze the dependence of the scale factor value on the inertial mass.

During the experiment, the thickness of the inertial masses in the matrix varied discretely. The output voltage at the electrodes of the secondary channel was estimated for each thickness value at different angular velocity values. The assessment was carried out at a step of 500 rad/s to a maximum value of 2000 rad/s, which corresponds to approximately 114650 deg/s. The thicknesses were 0.001, 0.5, 1, 2, 5 and 10 μm. Large thicknesses were not considered for the reason that such films are already difficult enough to process with a laser so that the geometry of the elements meets the necessary requirements. The results of the tests are shown in Fig. 11.
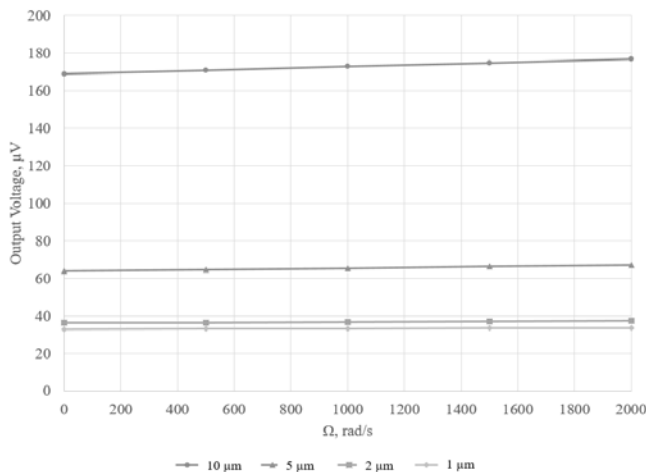


Fig. 11. Sensitivity of a gyro with different thickness of inertial masses

The graph shows that with an increase in the thickness of the inertial masses, the steepness of the output characteristic increases. In this case, the zero shift also increased from 32 to 170 µV. Its growth is probably due to the fact that with a larger thickness of the inertial masses, the scattering effects also increase. However, this is a positive moment, since large output voltages are easier to measure. At the same time, the nonlinear distortion coefficient attracts attention. Throughout the measurement range, its value is less than 0.1%. The values of scale factors for each inertial mass thickness are presented in Table 1.

Based on the obtained results, it can be concluded that an increase in the thickness of the inertial masses to 10 μm made it possible to increase the scale factor by an order of magnitude. This fact must be taken into account in the production of prototypes and choose a thicker metallization.

Comparing the results of computer simulation, as well as the spectrum of real samples obtained by laser deposition, we can calculate the parasitic zero shift (value of output signal with zero input). The data obtained from the spectrum analyzer state that the difference between the calculated and real frequencies is less than 1%. The attenuation at the frequency (central) of 16.49 MHz is -7.6 dB. In the case of an error of 1%, we obtain a frequency equal to 16.33 MHz. With this value attenuation will be -7 dB. If we recalculate this value into a voltage, we obtain an additional zero shift of $105.4 \cdot 10^{-9}$ V (for the case with an inertial mass thickness of 10 μm). This corresponds to an angular velocity $\Omega = 27.16$ rad/s, which the sensor will show when at rest. To eliminate this error, it is necessary to design sensors with a bandwidth of more than 1% of the carrier.

V. CONCLUSION

A prototype of a solid-state SAW-based gyro on standing waves was produced by laser ablation method and tested on a spectrum analyzer. Test results show that the central frequency error is less than 1% and produced resonator shows a narrow peak with small side harmonics. It shows that the method is suitable for quick prototyping of this type of sensors.

In addition, a finite element modeling was performed to find out the dependence between metallization thickness and the gyro scale factor. It was shown that thicker films are better from the sensitivity point of view. Created model may also be used for further optimization of topology geometrical parameters.

Further we plan to surround produced sensing element with a proper electrical circuit and test it as a model of a surface acoustic wave gyroscope.

REFERENCES

[1] Bo L. et al., "Surface acoustic wave devices for sensor applications", *Journal of Semiconductors*, №2, vol. 37, 2016, p.021001.

[2] Lukyanov D., Shevchenko S., Kukaev A., "Micro rate gyros for highly dynamic objects", *Microsystem technologies,* №12, vol. 20, 2014, pp. 2137-2146.

[3] Xu F. et al., "Optimization of surface acoustic wave-based rate sensors" *Sensors,* №. 10, vol. 15, 2015, pp. 25761-25773.

[4] Oh H. et al., "Enhanced sensitivity of a surface acoustic wave gyroscope using a progressive wave" *Journal of Micromechanics and Microengineering*, №. 7, vol. 21, 2011, pp. 075015.

[5] Mahmoud A. et al., "Investigating the impact of resonant cavity design on surface acoustic wave gyroscope" *Inertial Sensors and Systems (INERTIAL), 2018 IEEE International Symposium on.,* IEEE, 2018, pp. 1-4.

[6] Lukyanov D. et al., "Design and research of bidirectional surface acoustic wave delay line fabricated using laser ablation method", *Fiber Lasers and Glass Photonics: Materials through Applications. – International Society for Optics and Photonics*, vol. 10683, 2018, p. 106833O.

[7] Lukyanov D. et al., "Experimental study of laser trimmed surface acoustic wave delay line topologies" *Optical Sensors 2017*, SPIE, vol. 10231, 2017, p. 102311T.

[8] Kurosawa M. et al., "A surface-acoustic-wave gyro sensor" *Sensors and Actuators A: Physical.* №. 1-3, vol. 66, 1998, pp. 33-39.

[9] Jose K. A. et al., "Surface acoustic wave MEMS gyroscope", *Wave motion.* №. 4, vol. 36, 2002 pp. 367-381.

[10] D. Lukyanov et. al., Patent RU № 137098 "Microgyroscope on surface acoustic waves", January 2014.

[11] MiniMarker 2 technical characteristics, Web: http://www.minimarker.ru/tech_data.php